

Finite-temperature effects on the number fluctuation of ultracold atoms across the Superfluid to Mott-insulator transition

Xiancong Lu and Yue Yu

Institute of Theoretical Physics, Chinese Academy of Sciences, P.O. Box 2735, Beijing 100080, China

(Dated: August 29, 2018)

We study the thermodynamics of ultracold Bose atoms in optical lattices by numerically diagonalizing the mean-field Hamiltonian of the Bose-Hubbard model. This method well describes the behavior of long-range correlations and therefore is valid deep in the superfluid phase. For the homogeneous Bose-Hubbard model, we draw the finite-temperature phase diagram and calculate the superfluid density at unity filling. We evaluate the finite-temperature effects in a recent experiment probing number fluctuation [Phys. Rev. Lett. **96**, 090401 (2006)], and find that our finite-temperature curves give a better fitting to the experimental data, implying non-negligible temperature effects in this experiment.

PACS numbers: 03.75.Lm,03.75.Hh,67.40.-w

I. INTRODUCTION

The ultracold Bose atoms in optical lattices have opened a new window to investigate the strongly correlated systems with highly tunable parameters [1]. The basic physics of these ultracold atomic systems is captured by the Bose-Hubbard model, whose most fundamental feature is the existence of superfluid to Mott-insulator (MI) phase transition [2, 3]. In a shallow optical lattice, the ultracold atoms are in superfluid phase, which can be well-described by a macroscopic wave function with long-range phase coherence [4]. In this case, phase fluctuation vanishes and on-site number fluctuation diverges. Whereas, in a deep optical lattice, the atoms are in MI phase if the filling factor is fixed to an integer, leading to zero on-site number fluctuation and divergent phase fluctuation [4, 5].

The physics of the MI phase is that, when the repulsive interaction between atoms is large enough, the number fluctuation would become energetically unfavorable, forcing the system into a number-squeezed state. This interaction induced MI phase plays an important role in the strongly correlated systems, as well as various quantum information processing schemes [6]. In the past, a series of ultracold-atom experiments have been performed to detect this number-squeezed MI phase through the observation of increased phase fluctuations [4, 5, 7] or through an increased time scale for phase diffusion [8, 9].

Recently, a continuous suppression of on-site number fluctuation was directly observed by Gerbier *et al.* by monitoring the suppression of spin-changing collisions across the superfluid to Mott-insulator transition [9]. By using a far off-resonant microwave field, the spin oscillations for doubly occupied sites can be tuned into resonance, and its amplitude is directly related to the probability of finding atom pairs in a lattice site. It was shown by Gerbier *et al.* that, for a small atom number, the oscillation amplitude is increasingly suppressed when the lattice depth is increased and completely vanishes for sufficiently large lattice depth. They also compared the experimental results with the prediction of the

Bose-Hubbard model within a mean-field approximation at zero temperature. However, the theoretical curves at zero temperature do not fully fit with the experimental data, especially in low optical lattices. An important reason for this deviation is the neglect of finite-temperature effects in the calculation. This motivates us to study the finite-temperature properties of these ultracold atoms expecting a better fitting to the experimental data.

In the past, various theoretical approaches have been used to investigate the zero temperature properties of the Bose-Hubbard model such as the mean-field approximation [2, 10, 11], strong-coupling expansion [12], Gutzwiller projection ansatz [3, 13, 14], and quantum Monte Carlo simulation [15]. There are also a few works focusing on the finite-temperature properties of the Bose-Hubbard model, such as the standard basis operator method [10, 16], slave particle approach [17, 18], coarse-graining mean-field approximation [19], analytic investigation of fixed point [20], and some others [21, 22]. However, most of these approaches are based on the perturbation theory in terms of small superfluid order parameter and therefore are only valid near the superfluid to normal-liquid phase transition or in the Mott region. Recently, Oosten *et al.* have used an effective approach, which is a finite-temperature extension of the zero temperature mean field theory proposed by Sheshardi *et al.* [10], to study the thermodynamics of the system with large filling factor [23]. This mean-field theory correctly includes the long-rang correlations [14, 24] and thus is valid deep in the superfluid phase [25]. In this paper, we will use it to calculate the thermodynamic quantities from the high superfluid region to the normal-liquid (or MI) region.

This paper is organized as follows. In Sec. II, we will describe the finite-temperature mean-field theory for the Bose-Hubbard model. We will draw the finite-temperature phase diagram and investigate the system with unity filling factor. In Sec. III, we will calculate the finite-temperature number fluctuations and compare them with the experimental results of Ref. [9]. In Sec. IV, we will give our conclusions.

II. FINITE-TEMPERATURE MEAN-FIELD THEORY TO BOSE-HUBBARD MODEL

We consider an ultracold Bose atom gas confined in a three-dimensional optical lattice potential. In real experiments, a slow varying trapping potential is superimposed onto the lattice potential. We only pay attention to the homogeneous case in this section and will consider the trapping potential in the next section. The homogenous Bose atom system can be well-described by the following Bose-Hubbard Hamiltonian [3]:

$$H = -t \sum_{\langle ij \rangle} b_i^\dagger b_j - \mu \sum_i n_i + \frac{U}{2} \sum_i n_i(n_i - 1). \quad (1)$$

Here b_i^\dagger is the creation operator at site i , $n_i = b_i^\dagger b_i$ is the particle number operator, and $\langle ij \rangle$ denotes the sum over nearest neighbor sites. t and U are the hopping amplitude and on-site interaction, respectively. In the mean-field approximation [10], the hopping term is decoupled as

$$\begin{aligned} b_i^\dagger b_j &= \langle b_i^\dagger \rangle b_j + \langle b_j^\dagger \rangle b_i - \langle b_i^\dagger \rangle \langle b_j^\dagger \rangle \\ &= \phi(b_i^\dagger + b_j) - \phi^2, \end{aligned} \quad (2)$$

where $\phi = \langle b_i^\dagger \rangle = \langle b_i \rangle$ is the superfluid order parameter. The Hamiltonian of the Bose-Hubbard model can be written as a sum over single-site terms, $H = \sum_i H_i$, where

$$H_i = \frac{U}{2} n_i(n_i - 1) - \mu n_i - zt\phi(b_i^\dagger + b_i) + zt\phi^2, \quad (3)$$

with z being the number of nearest neighbors. In Ref. [10], Sheshardi *et al.* have studied the zero-temperature properties of the Bose-Hubbard model by diagonalizing the Hamiltonian H_i in the occupation number basis $\{|n\rangle\}$ truncated at a finite value n_t . Here, we will extend this method to include the temperature effects [23] and investigate the finite-temperature properties of the same model. We first obtain the matrix of H_i in the truncated occupation number basis, which has a symmetric tridiagonal form:

$$\begin{pmatrix} d(1) & e(1) & 0 & \dots & & 0 \\ e(1) & d(2) & e(2) & & & \vdots \\ 0 & e(2) & d(3) & & & \\ \vdots & & \vdots & & & \\ & & & d(n_t - 1) & e(n_t - 1) & 0 \\ & & & e(n_t - 1) & d(n_t) & e(n_t) \\ 0 & \dots & & 0 & e(n_t) & d(n_t + 1) \end{pmatrix}, \quad (4)$$

where the diagonal elements $d(k)$ and subdiagonal elements $e(k)$ are

$$d(k) = \frac{U}{2}(k-1)(k-2) - \mu(k-1) + zt\phi^2, \quad (5)$$

$$e(k) = -\sqrt{k}zt\phi, \quad (6)$$

and all other matrix elements are zero. We diagonalize this matrix to obtain the energy spectrum $\{E_k\}$ and eigenstates $|\psi_k\rangle$, and then evaluate the partition function and the free energy,

$$Z = \sum_{k=1}^{n_t+1} e^{-\beta E_k}, \quad F = -\frac{1}{\beta} \ln Z. \quad (7)$$

For given U , t , μ , and T , the superfluid order parameter ϕ can be determined by minimizing the free energy, i.e.,

$$\left. \frac{\partial F}{\partial \phi} \right|_{U,t,\mu,T} = 0. \quad (8)$$

The region with nonzero ϕ is identified as the superfluid phase while the region with $\phi = 0$ as the Mott-insulator or normal-liquid phase. After determining ϕ , it is easy to calculate other physical quantities such as the superfluid density ρ_s and average density ρ with

$$\rho_s = \phi^2, \quad \rho = \langle n \rangle = \frac{\text{Tr}(n e^{-\beta H})}{Z}. \quad (9)$$

We show our main results in Figs. 1 - 4. The finite-temperature phase diagrams are plotted in Fig. 1 in the μ/zt - U/zt plane. The different curves represent the phase boundaries between superfluid and normal liquid (or MI) at different temperatures. One can see that the zero-temperature Mott lobes are enlarged and disappear gradually with the increasing temperature. This is the so-called MI to normal-liquid crossover. We see that the crossover temperature is about $0.5 - 0.7zt$ around the first Mott lobe (red curves), while it is about $1.1 - 1.3zt$ around the second one (blue curves). Note that we set $k_B = 1$ throughout this work. The second Mott lobe is more stable against the temperature than the first because of the larger interaction U .

In Fig. 2, we show the average density ρ as a function of μ/zt for different temperatures and fixed interaction $U/zt = 12$. At zero temperature, there are plateaus on the curve with integer filling factor and zero compressibility. When increasing the temperature, these plateaus are shrunk and eventually disappear. The qualitative behaviors of all these curves are the same as those of previous finite-temperature works based on perturbation theory [16, 17, 18, 19]. However, our results persist deep into the superfluid phase.

We then turn to investigate the system with an integer filling factor, $\rho = 1$, at which the superfluid to Mott-insulator phase transition may occur. The evolution of superfluid density as a function of interaction at different temperatures is shown in Fig. 3. At zero temperature, ρ_s drops to zero at a critical interaction $U_c/zt = 5.83$, in good agreement with the analytical result [11]. When increasing the temperature, the superfluid density as well as the critical interaction is reduced. Both of them vanish when T/zt is larger than 1.45. We record the critical

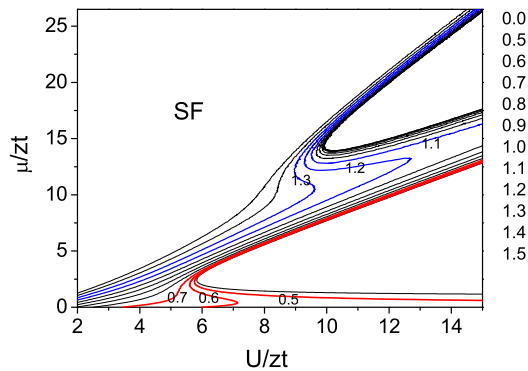


FIG. 1: (Color online) The finite-temperature phase diagram of the Bose-Hubbard model in the μ/zt - U/zt plane. The temperature is increasing when evolving away from the zero-temperature Mott lobes. The temperature T/zt of each curve is listed in a column on the right side of the figure. The red curves with values 0.5, 0.6, and 0.7 on them indicate the crossover region for the first Mott lobe, and the blue ones with 1.1, 1.2, and 1.3 on them indicate the crossover for the second lobe.

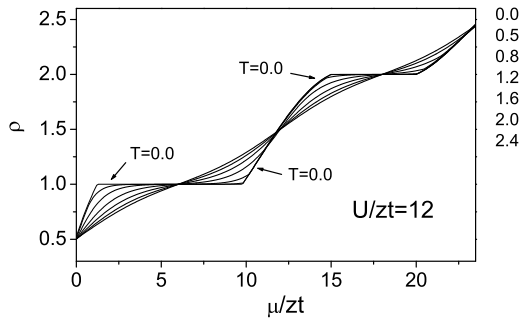


FIG. 2: Average density ρ as a function of μ/zt at a fixed interaction $U/zt = 12$. The temperature is increasing when evolving away from the zero-temperature curve, which is indicated by the arrows in the figure. We list the temperature of each curve in the column on the right side of the figure.

interaction for every temperature, and plot inversely the critical temperature T_c/zt as a function of interaction in the inset. This is consistent with our previous result in Ref. [18].

In Fig. 4, we show the probability $P(2)$ of a site to be doubly occupied as a function of interaction U/zt for different temperatures. At zero temperature, there is an obvious suppression of $P(2)$ with the increasing interaction, i.e., $P(2)$ reduces to zero when entering the MI region. However, one can see that the suppression is weakened as the temperature is increased. This phenomenon has recently been observed by Gerbier *et al.* by using a spin-

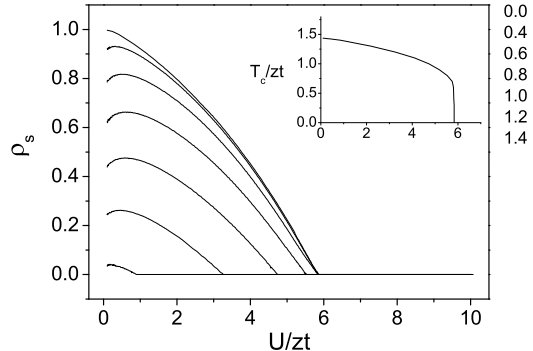


FIG. 3: Superfluid density ρ_s vs interaction U/zt for different temperatures in the case of integer filling $\rho = 1$. The temperature of each curve is increasing from up to down, with their values listed in the column on the right side. In the inset, the critical temperature T_c/zt of the phase transition is plotted as a function of interaction U/zt .

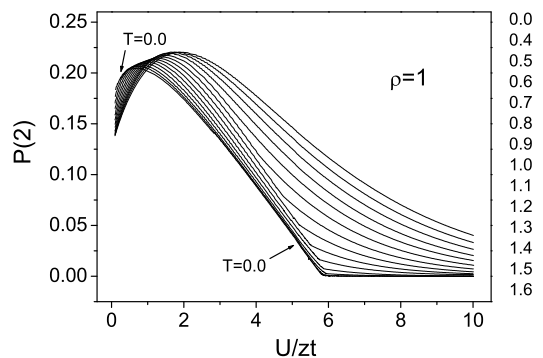


FIG. 4: Probability $P(2)$ of a site to be doubly occupied vs interaction U/zt for different temperatures, with fixing filling factor $\rho = 1$. The temperature of each curve is decreasing from up to down, with their values listed on the right side as usual.

changing collision technique [9]. We will discuss this in detail in the next section.

In the final of this section, we evaluate the effect of finite truncation to the occupation number basis. As we know, the smaller U/zt the larger n_t is needed for small error [10]. We then plot in Fig. 5 the superfluid densities ρ_s of a unity filling system versus the truncation n_t for a very small interaction $U/zt = 0.2$. One can see that the finite-truncation approximation is quite worse in the small n_t region, i.e., the magnitude of ρ_s with n_t is quite different from that with $n_t + 1$. This finite-truncation effect is strengthened when increasing the temperature. However, when n_t is larger than 6, it becomes very small even for a high temperature. Typically, the difference of

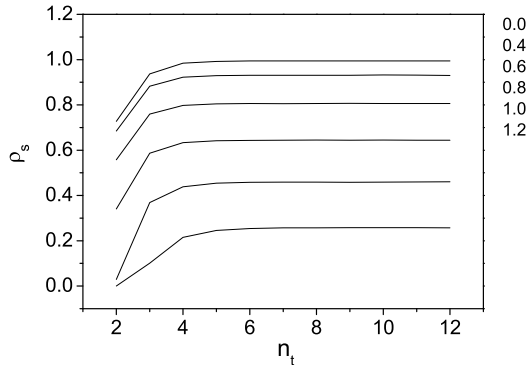


FIG. 5: Superfluid density ρ_s vs truncation n_t for different temperatures. The density is $\rho = 1$ and the interaction is $U/zt = 0.2$. The temperature of each curve is increasing from up to down, with their values listed on the right.

ρ_s between $n_t = 10$ and $n_t = 11$ is smaller than 0.5%, which means the effect of finite truncation is very small. Therefore we choose $n_t = 10$ in all of our calculations.

III. THE FINITE-TEMPERATURE NUMBER FLUCTUATIONS: COMPARING TO EXPERIMENT

In this section, we will evaluate the finite-temperature number fluctuations of ultracold atoms in optical lattices and compare them with the experimental data in Ref. [9]. The ultracold atomic gas is confined in a three-dimensional optical lattice potential $V_{OL}(\mathbf{r})$ with

$$V_{OL}(\mathbf{r}) = V_0 \sum_{j=1}^3 \sin^2(kr_j), \quad (10)$$

where V_0 is the lattice depth, $k = 2\pi/\lambda$ is the wave vector with λ being the laser wavelength. In addition, the atomic gas is also subjected to a trapping potential $V_{ext}(\mathbf{r})$, which can be approximately considered as a harmonic one [26],

$$V_{ext}(\mathbf{r}) = \frac{1}{2}m\omega^2\mathbf{r}^2, \quad (11)$$

with the trapping frequency given by

$$\omega = \sqrt{\omega_m^2 + \frac{8V_0}{mw^2}}. \quad (12)$$

Here m is the atom mass, ω_m is the frequency of the magnetic trap where the condensate is initially formed, and w is the waist of the lattice beams [9, 26]. If this trapping potential is very shallow and varies slowly across the atomic cloud, we can treat it within the local density approximation (for more details, see Ref. [26]).

We now specify the values of the parameters used in our calculations. The hopping amplitude t and on-site interaction U of the Bose-Hubbard model can be determined by

$$t = \int d\mathbf{r} w^*(\mathbf{r} - \mathbf{r}_i) \left(-\frac{\hbar^2}{2m} \nabla^2 + V_{OL}(\mathbf{r}) \right) w(\mathbf{r} - \mathbf{r}_j), \quad (13)$$

$$U = \frac{4\pi a_s \hbar^2}{m} \int d\mathbf{r} |w(\mathbf{r})|^4, \quad (14)$$

where a_s is the s-wave scattering length and $w(\mathbf{r})$ is the Wannier function. Here, we use the approximate expressions [26]

$$\frac{t}{E_r} = 1.43 \left(\frac{V_0}{E_r} \right)^{0.98} \exp(-2.07\sqrt{V_0/E_r}), \quad (15)$$

$$\frac{U}{E_r} = 5.97 \left(\frac{a_s}{\lambda} \right) \left(\frac{V_0}{E_r} \right)^{0.88}, \quad (16)$$

where $E_r = \hbar^2/2m\lambda^2$ is the single-photon recoil energy. The triplet scattering length for the ^{87}Rb atom is $a_s = 5.61$ nm [27], the laser wavelength $\lambda = 842$ nm, the lattice spacing $d = \lambda/2 = 421$ nm, the magnetic trapping frequency $\omega_m = 2\pi \times 16$ Hz, and the waist $w = 136$ μm . All these values coincide exactly with those in the real experiment [9].

We show in Fig. 6 the density distribution of ultracold atomic gas with total number $N = 1.0 \times 10^5$ in two typical optical lattice depths. We can see that, at zero-temperature and in the low optical lattice [Fig. 6(a)], the density decreases smoothly when leaving the center of the trap. However, a Mott-shell structure forms in the deep lattice [Fig. 6(b)]. When increasing the temperature, the atomic cloud is expanding and the Mott-plateaus in the deep lattice are melting gradually. Most recently, the formation of Mott-shell structure is directly observed [28, 29]. The calculation of the finite-temperature effects in these experiments is ongoing.

We now turn to the number fluctuation experiment performed by Gerbier *et al.* [9]. In explaining their experimental results, the authors used a zero-temperature mean-field theory, which gives the correct trend. However, they also found some discrepancies, especially in the low lattice depths [9]. We find that these discrepancies can be diminished by taking the finite-temperature effect into account. We show the probability $\bar{P}(2)$ of finding atoms in the doubly occupied sites, averaged over the whole atomic cloud, in Fig. 7 as a function of total atom number N for different lattice depths and temperatures. The zero temperature curve in each panel coincides with the theoretical estimate in Ref. [9]. One can see that their deviation from the experimental data, which are denoted by circles in the figure, is quite obvious. In panel (a) where the atoms are in superfluid phase, $\bar{P}(2)$ always decreases with the increasing temperature. When comparing with the experimental data, we can see that for

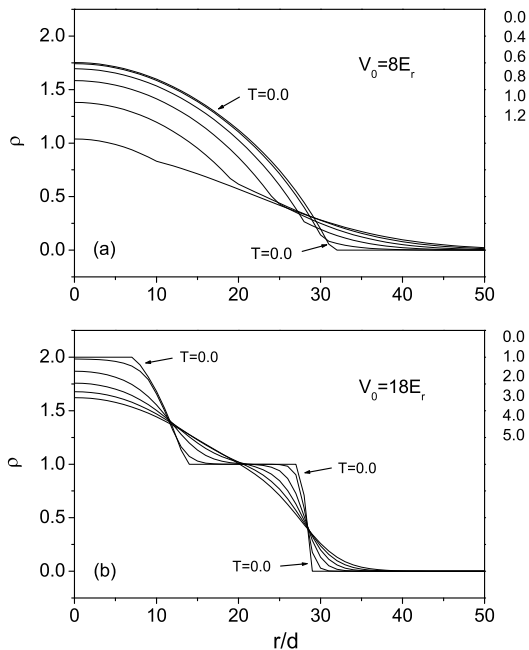


FIG. 6: Density distribution of ultracold atom gas with a total atom number $N = 1.0 \times 10^5$ in different optical lattice depths $V_0 = 8E_r$ (a) and $V_0 = 18E_r$ (b). The zero-temperature curves are indicated by arrows in the figure. The temperature of each curve is increasing when evolving away from the zero-temperature one, with their values listed in the columns on the right side.

small atom number the discrepancy between the zero-temperature curve and the experimental data can be reduced by taking the temperature into account. In panel (b), we observe that the finite-temperature curve with a proper temperature, e.g., the red curve with $T/zt = 0.7$, agrees well with the experimental data in the whole range of N . In panel (c) where the atoms are near the superfluid to Mott-insulator transition, the influence of the temperature is a little complex. In the small N region, $\bar{P}(2)$ first decreases and then increases with the increasing temperature. The decrease at the beginning is due to the suppression of superfluid density by the temperature, and the following increase is caused by the temperature exciting more atoms to occupy the eigenstate $|2\rangle$. In the large N region, however, the behavior of $\bar{P}(2)$ is inverse: it first increases and then decreases with the increasing temperature. Again, we find that the curve with high temperature (e.g., the red curve with $T/zt = 1.5$) fits fairly well with the experimental data. In panel (d) where the atoms are deep in the Mott region, the amplitude of $\bar{P}(2)$ is improved in the small N region, but is suppressed in the large N region, as the temperature increases. This behavior is consistent with the experimental data too. The investigation of these finite-temperature effects has its own interest, for it provides a possible way to esti-

mate the temperature of the atomic gas [28]. In our case, $1.0zt$ yields several ten nano-Kelvin and the temperature regime where the experimental data located in is $10^1 \sim 10^2$ nK, therefore our estimate to temperature is quite reasonable.

Before closing this section, we observe that, in the large N region, there are still some inconsistencies between our results and the experimental data. Within the deep superfluid regime [Fig. 7(a)], $\bar{P}(2)$ is always smaller than the experimental data in the large N region. A possible reason for this discrepancy is the large probability for triplet occupation, which is due to the high density in the center of the trap ($\rho \approx 3$) and the large number fluctuation of the system in so low lattice potential. In experiment, the presence of large triplet occupation may change the spin resonance condition, resulting in a considerable contribution of spin oscillations on triply occupied sites to the observed oscillation amplitude [9, 30]. This makes the experimental measurements larger than the calculated $\bar{P}(2)$ (see also Fig. 4 of Ref. [9]). Within the deep MI regime [Fig. 7(d)], our finite-temperature consideration does give a correct trend in the large N region. However, the reason for the further suppression of oscillation amplitude is not uncovered yet, which cannot be simply attributed to the temperature effects.

IV. CONCLUSIONS

We studied the finite-temperature properties of the Bose-Hubbard model by numerically diagonalizing the mean-field Hamiltonian on a truncated occupation number basis. This method can give the thermodynamics deep in the superfluid phase. For the homogenous Bose-Hubbard model, we calculated the finite-temperature phase diagram and plotted the density versus chemical potential curve. We demonstrated the evolution of zero-temperature Mott lobes and Mott plateaus when the temperature is increasing. We then specially investigated the system with unity filling factor. The superfluid density and the probability $P(2)$ of finding a site to be doubly occupied were plotted as a function of interaction. We found that the superfluid density is reduced and the suppression of $P(2)$ is weakened as the temperature increases. In the second part of this paper, we evaluated the finite-temperature effects in a recent experiment probing the number fluctuation [9]. We showed that the calculated finite-temperature curves fit the experimental data better than the zero-temperature ones. This implies that the finite-temperature effects in this experiment are quite large.

Acknowledgments

We thank Fabrice Gerbier for a lot of useful discussions and explaining their experimental and theoretical results. We are also grateful to Jingyu Gan, Liang He, Shijie

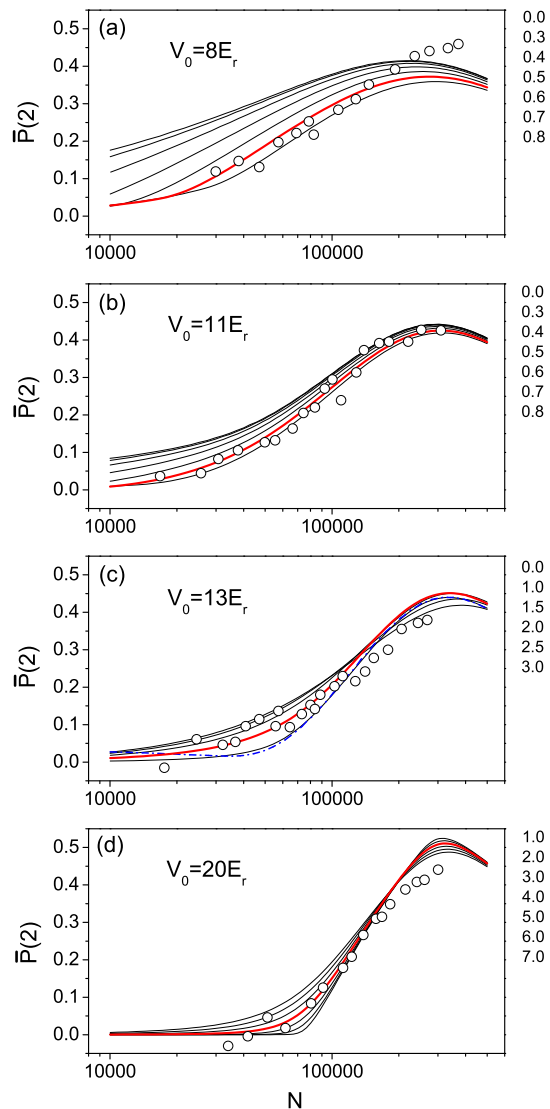


FIG. 7: (Color online) The probability $\bar{P}(2)$ of finding atoms in the doubly occupied sites, averaged over the whole atomic cloud, vs the total atom number N for different lattice depths. The circles are the experimental results reproduced from Ref. [9]. In panels (a) and (b), the temperature of each curve is increasing from up to down. In panel (c), the blue dash-dot curve corresponds to $T/zt = 0.0$. For other curves, the temperature is decreasing from up to down in the small N region, but is increasing from up to down in the large N region. Panel (d) has a similar temperature trend. From up to down, the temperature is decreasing in the small N region but is increasing in the large N region. As usual, the value of temperature is listed on the right side of each panel. The temperatures of the red curves in panels (a), (b), (c), and (d) are $T/zt = 0.7, 0.7, 1.5,$ and 4.0 , respectively.

Hu, Yuchuan Wen, Shijie Yang, and Hao Yin for helpful discussions. This work was supported in part by Chinese National Natural Science Foundation.

[1] I. Bloch, Phys. World, **17**, 25 (2004); I. Bloch, Nat. Phys. **1**, 23 (2005).

[2] M. P. A. Fisher, P. B. Weichman, G. Grinstein, and D.

- S. Fisher, Phys. Rev. B **40**, 546 (1989).
- [3] D. Jaksch, C. Bruder, J. I. Cirac, C. W. Gardiner, and P. Zoller, Phys. Rev. Lett. **81**, 3108 (1998).
- [4] M. Greiner, O. Mandel, T. Esslinger, T. W. Hänsch, and I. Bloch, Nature (London) **415**, 39 (2002).
- [5] C. Orzel, A. K. Tuchman, M. L. Fenselau, M. Yasuda, and M. A. Kasevich, Science **291**, 2386 (2001).
- [6] P. Rabl, A. J. Daley, P. O. Fedichev, J. I. Cirac, and P. Zoller, Phys. Rev. Lett. **91**, 110403 (2003); G. Pupillo, A. M. Rey, G. K. Brennen, C. W. Clark, and C. J. Williams, J. Mod. Opt. **51**, 2395 (2004).
- [7] T. Stöferle, H. Moritz, C. Schori, M. Köhl, and T. Esslinger, Phys. Rev. Lett. **92**, 130403 (2004).
- [8] M. Greiner, O. Mandel, T. W. Hänsch, and I. Bloch, Nature (London) **419**, 51 (2002).
- [9] F. Gerbier, S. Fölling, A. Widera, O. Mandel, and I. Bloch, Phys. Rev. Lett. **96**, 090401 (2006).
- [10] K. Sheshardi *et al.*, Europhys. Lett. **22**, 257 (1993).
- [11] D. van Oosten, P. van der Straten, and H. T. C. Stoof, Phys. Rev. A **63**, 053601 (2001).
- [12] J. K. Freericks and H. Monien, Europhys. Lett. **26**, 545 (1994); J. K. Freericks and H. Monien, Phys. Rev. B **53**, 2691 (1996); N. Elstner and H. Monien, Phys. Rev. B **59**, 12184 (1999); K. Sengupta and N. Dupuis, Phys. Rev. A **71**, 033629 (2005).
- [13] W. Krauth, M. Caffarel, and J.-P. Bouchaud, Phys. Rev. B **45**, 3137 (1992); D. S. Rokhsar and B. G. Kotliar, Phys. Rev. B **44**, 10328 (1991).
- [14] C. Schroll, F. Marquardt, and C. Bruder, Phys. Rev. A **70**, 053609 (2004).
- [15] G. G. Batrouni, V. Rousseau, R. T. Scalettar, M. Rigol, A. Muramatsu, P. J. H. Denteneer, and M. Troyer, Phys. Rev. Lett. **89**, 117203 (2002); G. G. Batrouni, R. T. Scalettar, and G. T. Zimanyi, Phys. Rev. Lett. **65**, 1765 (1990); S. Wessel, F. Alet, M. Troyer, and G. G. Batrouni, Phys. Rev. A **70**, 053615 (2004).
- [16] S. Konabe, T. Nikuni, and M. Nakamura, Phys. Rev. A **73**, 033621 (2006); Y. Ohashi, M. Kitaura, and H. Matsumoto, Phys. Rev. A **73**, 033617 (2006).
- [17] D. B. M. Dickerscheid, D. van Oosten, P. J. H. Denteneer, and H. T. C. Stoof, Phys. Rev. A **68**, 043623 (2003).
- [18] Y. Yu and S. T. Chui, Phys. Rev. A **71**, 033608 (2005); X. C. Lu, J. B. Li, and Y. Yu, Phys. Rev. A **73**, 043607 (2006).
- [19] A. P. Kampf and G. T. Zimanyi, Phys. Rev. B **47**, 279 (1993).
- [20] P. Buonsante and A. Vezzani, Phys. Rev. A **70**, 033608 (2004).
- [21] B. DeMarco, C. Lannert, S. Vishveshwara, and T.-C. Wei, Phys. Rev. A **71**, 063601 (2005).
- [22] L. I. Plimak, M. K. Olsen, and M. Fleischhauer, Phys. Rev. A **70**, 013611 (2004); K. P. Schmidt, A. Reischl, and G. S. Uhrig, Eur. Phys. J. D **38**, 343 (2006).
- [23] D. van Oosten, P. van der Straten, and H. T. C. Stoof, Phys. Rev. A **67**, 033606 (2003).
- [24] J. J. Garcia-Ripoll *et al.*, Opt. Express **12**, 42 (2004).
- [25] Note that, although the mean field theory correctly includes the long-rang correlations, it does fail to describe the short-rang correlations between different lattice sites, which, however, can be obtained by the perturbation theory [14, 26]. Also note that this comparison is performed for the homogeneous system.
- [26] F. Gerbier, A. Widera, S. Fölling, O. Mandel, T. Gericke, and I. Bloch, Phys. Rev. A **72**, 053606 (2005); Phys. Rev. Lett. **95**, 050404 (2005).
- [27] C. J. Pethick and H. Smith, *Bose-Einstein Condensation in Dilute Gases* (Cambridge University Press, Cambridge, England, 2002).
- [28] S. Fölling, A. Widera, T. Müller, F. Gerbier, and I. Bloch, Phys. Rev. Lett. **97**, 060403 (2006).
- [29] G. K. Campbell, J. Mun, M. Boyd, P. Medley, A. E. Leanhardt, L. G. Marcassa, D. E. Pritchard, and W. Ketterle, Science **313**, 649 (2006).
- [30] B. Capogrosso-Sansone, E. Kozik, N. Prokof'ev, and B. Svistunov, cond-mat/0609600